

Influence of the Gas–Liquid Separator Design on Hydrodynamic and Mass Transfer Performance of Split-Channel Airlift Reactors

Keun H. Choi, Yusuf Chisti* & Murray Moo-Young

Department of Chemical Engineering, University of Waterloo, Waterloo, Ontario, Canada N2L 3G1

(Received 2 August 1994; accepted 28 September 1994)

Abstract: Three geometric configurations of gas–liquid separators were used in split-channel airlift reactors (0.1 m³ liquid volume; riser-to-downcomer cross-sectional area ratio = 0.7; aspect ratio = 3.6) to test the effect of geometry on hydrodynamic performance and oxygen transfer behaviour. For otherwise fixed conditions, the design of gas–liquid separators affected the induced liquid circulation rate, the depth of penetration of the bubble layer in the downcomer, the gas holdup in the downcomer, the mixing time and the overall volumetric gas–liquid oxygen transfer coefficient. The gas holdup in the riser was only marginally affected by the design of the separator. The impact of the various separator designs on hydrodynamic behaviour could be explained as emanating from a combination of the gas–liquid separating ability of the design and its hydraulic resistance.

Key words: airlift reactor, gas–liquid separator, hydrodynamics, oxygen transfer, wastewater treatment.

NOTATION

H_P	Bubble penetration depth (m)
$k_L a_L$	Overall volumetric oxygen transfer coefficient (s ⁻¹)
t_m	Mixing time (s)
T	Temperature (°C)
U_{Gr}	Superficial gas velocity based on riser cross-sectional area (m s ⁻¹)
U_{Ld}	Superficial liquid velocity in downcomer (m s ⁻¹)
α	Coefficient in eqn (2) (m ^{-β} s ^{β})
β	Exponent in eqn (2)
γ	Coefficient in eqn (3) (m ^{-δ} s ^{$\delta-1$})
δ	Exponent in eqn (3)
ϵ_G	Overall gas holdup
ϵ_{Gd}	Gas holdup in downcomer
ϵ_{Gr}	Gas holdup in riser

1 INTRODUCTION

The many attractive features of airlift reactors have led to increasing usage of these devices in environmental remediation technology, the chemical process industry and the biotechnology-based manufacture.^{1,2} Airlift reactors have an established niche in high-strength activated sludge type treatment of wastewater where the high oxygen transfer capability, low power requirements and non-mechanical agitation are particular advantages of these systems.^{1,3,4} Bioremediation of soil fines in airlift devices is being investigated as a promising new pollution abatement application of this technology.⁵ Similarly, applications in treatment of gaseous effluents are expected.⁶

An airlift reactor consists of a riser and a downcomer that are interconnected near the top and the bottom of the reactor as shown in Fig. 1. The riser is usually sparged with a gas, commonly air. The downcomer is usually not aerated. Differential aeration causes higher

* To whom correspondence should be addressed.

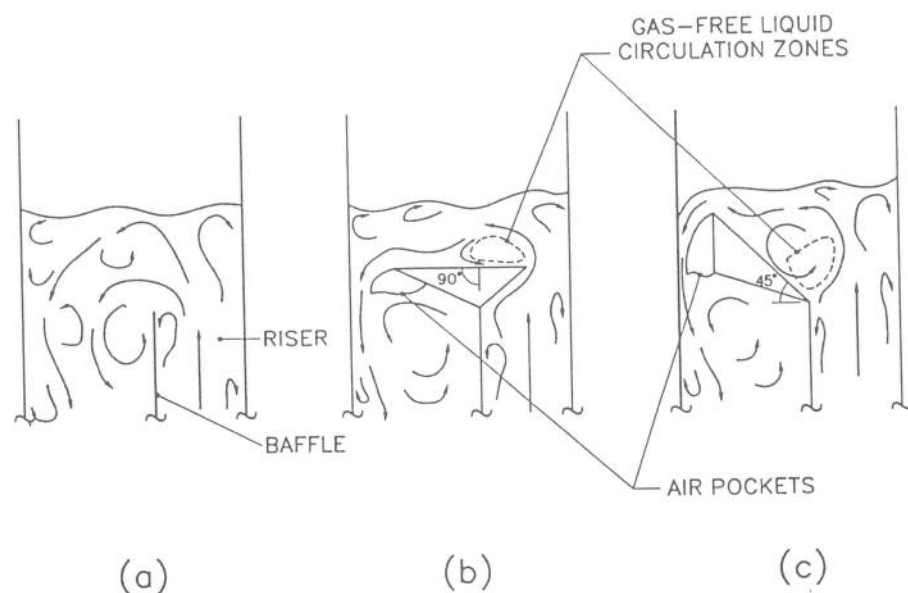


Fig. 2. Configurations of the head region: (a) without prism; (b) with a horizontal prism; (c) with a 45° inclined prism.

alternatively injected into the bottom of the downcomer as tracers. The variations in pH were monitored with a pH probe, pH meter and chart recorder arrangement. The pH probe was installed 1.29 m above the gas sparger in the riser. The mixing time was calculated from the response curves as the time required to achieve 90% of the final tracer concentration.

The overall volumetric oxygen transfer coefficient, $k_L a_L$, was determined by the dynamic gassing-in method as used previously by Chisti and Moo-Young.⁸ A polarographic dissolved oxygen electrode (Yellow Springs, YSI 5739) and a dissolved oxygen meter (YSI model 57) were used to follow the change in concentration of oxygen in a batch of liquid that had previously been freed of oxygen by bubbling through with nitrogen. The mass transfer coefficient data presented here has been corrected to a common temperature of 20°C using the equation:⁹

$$(k_L a_L)_{20} = \frac{(k_L a_L)_T}{(1.024)^{T-20}} \quad (1)$$

where the subscripts T and 20 denote values at any measurement temperature T and at 20°C, respectively.

3 RESULTS AND DISCUSSION

The general, visually observed, flow patterns in the three configurations of the head region are depicted in Fig. 2. In configuration (a) (Fig. 2), a local liquid circulation zone occurred just inside the downcomer, close to the upper edge of the baffle. As the liquid flow velocity increased, the flow separated from the edge of the baffle and a pocket of air, attached to the upper edge of the

baffle, formed inside the downcomer. A similar observation was previously reported for a different configuration of an airlift device.¹⁰ In configuration (c), particularly at low values of the riser superficial gas velocities (gas velocity below 0.049 m s^{-1}), most of the fluid that reached the narrow downcomer entrance was free of gas bubbles. However, because of the high velocity of local flow in the narrow entrance, any bubbles present were easily dragged into the downcomer. An air pocket formed on the downstream side of the prism, as shown in Fig. 2(b). Underneath the prism, in the downcomer, a large liquid circulation zone existed, but the intermixing between this zone and the bulk flow did not take place. A similar zone formed in configuration (c), but mixed relatively poorly with the rest of the flow. A large liquid circulation zone also existed above the prism in configuration (c) and a portion of this zone was free of gas bubbles (dotted lines in Fig. 2(c)). Interchange of fluid between the circulation zone and the bulk flow proceeded slowly. Unlike in configuration (c), the upper circulation zone in configuration (b) was quite small and better mixed; here too a gas-free zone, albeit smaller, existed. The air pocket in configuration (c) (Fig. 2) was larger than in configurations (a) or (b). The pocket occupied a large volume of the entrance zone in the downcomer. This entrance effect led to a higher downward liquid velocity near the outer edge of the downcomer than elsewhere within it. Thus, gas bubbles moved downward in this outer zone near the wall. Further away from the outer wall, the bubble could be seen to rise in the downcomer and disengage into the air pocket.

As illustrated in Fig. 3, the gas holdup in the riser was little affected by the configuration of the head region; however, the holdup in the downcomer was strongly affected. As expected, configuration (a) (Fig. 2)

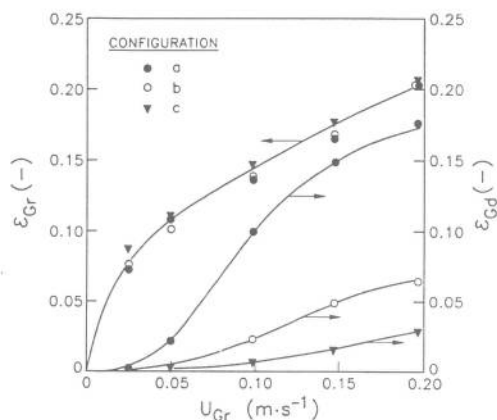


Fig. 3. Effects of the geometry of the head region on fractional gas holdups in the riser (ϵ_{Gr}) and the downcomer (ϵ_{Gd}).

was the least effective gas-liquid separator and allowed the greatest carryover of the gas bubbles into the downcomer, thus producing the highest downcomer gas holdup for any given conditions (Fig. 3). Configurations (b) and (c) in Fig. 2 were increasingly better in gas-liquid separating ability; consequently, the downcomer gas holdups were lower with these designs (Fig. 3). As is clear in Fig. 3, for any given operating gas velocity, the difference between the riser and downcomer gas holdups for various head region configurations increased in the order (c) > (b) > (a). Thus, the driving force for liquid circulation increased in the same order. Yet, in Fig. 4, for identical gas flow rates, the magnitude of the superficial liquid velocity in the downcomer followed an opposite trend, (a) > (b) > (c). Hence, configurations (a), (b) and (c) were achieving gas-liquid separation primarily by slowing down the circulation of the liquid, allowing the gas bubbles an increasing amount of time to disengage. The apparently anomalous combination of reduced liquid circulation rate and higher driving force, implies that the hydraulic resistance to liquid flow increased with the installation of the prisms in configuration (a) to obtain configu-

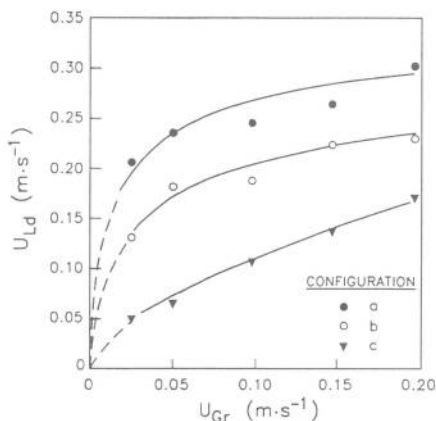


Fig. 4. Effects of the geometry of the head region on the induced superficial liquid velocity (U_{Ld}) in downcomer.

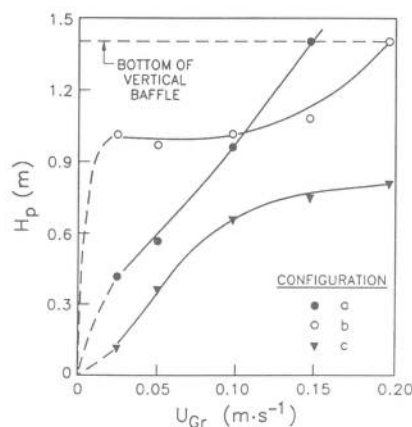


Fig. 5. Effects of the geometry of the head region on the depth of penetration (H_p) of the bubble front in the downcomer.

rations (b) and (c). The hydraulic resistance, or pressure drop, associated with designs (b) and (c) was caused by energy losses that arose because of the restricted flow paths. Further, the hydrodynamics of the flow around the prisms (configurations (b) and (c)) allowed significantly greater flow separation and formation of air pockets than occurred in design (a) (Fig. 2). Energy losses also took place in the circulating fluid zones which formed up- and down-stream of the prisms (Fig. 2(b and c)).

The effects of the geometry of the head region on bubble penetration depth in the downcomer are shown in Fig. 5 as a function of the superficial gas velocity in the riser. For the purpose of this work, the bubble penetration depth (H_p) is defined as the distance from the top of the vertical baffle to the bubble layer front in the downcomer. Although, for all three configurations, very small bubbles (approximately <2 mm diameter) did recirculate through the downcomer, such recirculation was disregarded in measurements of the bubble penetration depth. The latter referred to penetration of bubbles larger than about 3 mm. As shown in Fig. 5, the bubble penetration depth increased as the gas velocity increased. Similar results were reported by Fan *et al.*¹¹ in a three-phase concentric draft tube airlift reactor and by Chisti and Moo-Young¹⁰ in a rectangular channel airlift device having a different design from the ones used here. For configurations (a) and (b), at sufficiently large values of the gas velocity, the bubble front could reach the bottom of the vertical baffle. Recirculation of gas was achieved beyond this critical gas velocity, as was also observed by Fan *et al.*¹¹ However, in configuration (c), with a 45° inclined prism, bubble recirculation was not achieved in the range of gas velocities examined because of the relatively large pressure drop associated with that configuration. The critical gas velocity for configuration (a) was lower than that for configuration (b). This difference was directly related to the difference in relative magnitudes of liquid circulation rates in the two configurations.

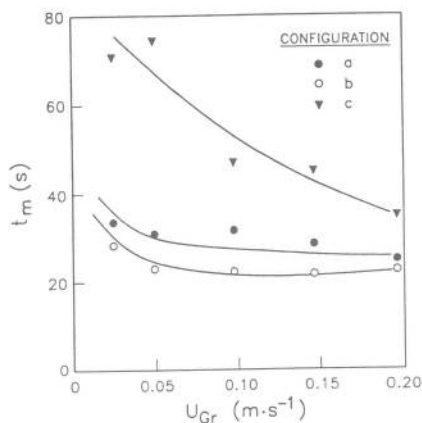


Fig. 6. Effects of the configuration of the head region on mixing time (t_m).

The rapid rise in bubble penetration depth that accompanied the initiation of gas flow in configuration (a) (dashed line in Fig. 5) again attested to the relatively low pressure drop offered by this configuration. Thus, slight increase in gas flow rate caused a large increase in liquid circulation rate (see also Fig. 4); an earlier onset of bubble flow into downcomer occurred and the bubbles penetrated deeper into the downcomer.

The relatively high depth of penetration at low gas velocities that was observed in configuration (b) (Fig. 5) was caused by the relatively high local superficial liquid velocity in the narrow entrance of the downcomer. This high local flow was capable of dragging any gas bubble that reached this zone into the downcomer. Once substantial gas holdup had been attained in the downcomer, further increase in gas flow did not increase the driving force for liquid circulation; thus, further increases in bubble penetration depth (Fig. 5) were not as spectacular. In configuration (c) although the local flow in the narrow downcomer entrance could be of similar magnitude to that in configuration (b), most of the gas bubbles had already escaped the liquid by the time the flow reached the narrow entrance.

The effects of the geometry of the head zone on mixing time are shown in Fig. 6. As expected, irrespective of the geometry of the upper region, the mixing time decreased with increasing superficial gas velocity. The specific power input to the reactor increased with increased gas flow; hence, turbulence and backmixing became more intensive as the liquid circulation also increased. Configuration (c) had the poorest mixing performance (Fig. 6) because of relatively low velocities of induced liquid circulation and the large eddy recirculation zones (Fig. 2(c)). The intermixing between the recirculation zones and the bulk flow was slow. The mixing performance of configurations (a) and (b) were similar; although, unexpectedly, configuration (b) was a consistently better mixer (shorter mixing times) than configuration (a). For identical energy input or superficial gas velocities in the two configurations,¹⁰ configuration (a)

TABLE 1
Constants in Eqns (2) and (3) for Various Configurations of the Head Region

Configuration	α	β	γ	δ
(a)	0.7426	0.8167	0.2289	0.7847
(b)	0.6008	0.7517	0.1987	0.0832
(c)	0.5271	0.7340	0.2690	0.1015

produced greater bulk liquid circulation because of its hydrodynamically smoother liquid circulation pathway (Fig. 4). Most of the energy imparted to the liquid went into creating the primary circulatory flow, but not so much into generating secondary eddies that enhance mixing. In configuration (b), with a relatively greater hydrodynamic resistance to primary circulatory flow, a larger proportion of the energy went into secondary flow systems; thus improving the mixing performance relative to configuration (a). This behaviour arose, because, despite the secondary flow systems in configuration (b), the volume of stagnant zones was limited in comparison with configuration (c).

Because of the effects of gas-liquid separator configuration on the downcomer gas holdup, for otherwise equal conditions, the overall gas holdup decreased in order (a) > (b) > (c). The overall gas holdups were correlated with the superficial gas velocity in the riser using the equation:

$$\varepsilon_G = \alpha U_{Gr}^\beta \quad (2)$$

The values of α and β for various head zone configurations are summarized in Table 1. The fundamental hydrodynamic basis of eqn (2) has been explained previously.¹²

The data on the overall volumetric oxygen transfer coefficient for the three configurations are presented in Fig. 7. In all cases, as the superficial gas velocity increased, the overall volumetric oxygen transfer coefficient

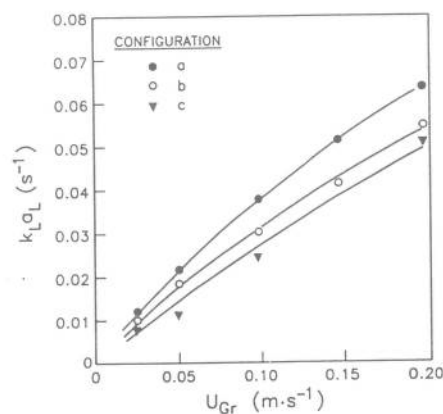


Fig. 7. Effects of the configuration of the head region on the overall volumetric oxygen transfer coefficient ($k_L a_L$).

cient, $k_L a_L$, increased because of an increase in the overall gas holdup and, hence, an increase in the gas-liquid interfacial area for oxygen transfer. The $k_L a_L$ values in configuration (a) were the greatest because this configuration produced the largest values of the overall gas holdup. The oxygen transfer coefficient data could be correlated with the superficial gas velocity using the equation:

$$k_L a_L = \gamma U_{Gr}^\delta \quad (3)$$

The values of γ and δ for various configurations of the separator zone are summarized in Table 1.

4 CONCLUSION

The hydrodynamic and aeration performance of split-channel internal-loop airlift reactors was shown to depend on the geometric configuration of the gas-liquid separator zone. For otherwise fixed conditions—aspect ratio of reactor, riser-to-downcomer cross-sectional area ratio and operational gas velocity—the performance characteristics, including the velocity of the induced liquid circulation, gas holdup in the downcomer, depth of penetration of the bubble front in downcomer, mixing time and the overall volumetric gas-liquid oxygen transfer coefficient, could be manipulated through design of the head zone. However, the gas holdup in the riser was not sensitive to the geometry of the head region. The effects of any geometric configuration on performance characteristics could be explained as originating from a combination of the gas-liquid separating ability of the configuration and its hydraulic resistance. Empirical correlations were proposed for estimation of the overall gas holdup and the overall volumetric oxygen transfer coefficient in an air-water system for three configurations of gas-liquid separators for potential use in wastewater treatment applications.

ACKNOWLEDGEMENTS

This work was funded by the Natural Sciences and Engineering Research Council of Canada. One of the authors (KHC) was supported by the Korea Science and Engineering Foundation.

REFERENCES

1. Chisti, Y., *Airlift Bioreactors*. Elsevier Applied Science, London, 1989.
2. Onken, U. & Weiland, P. Airlift fermenters: construction behaviour and uses. In *Adv. Biotechnol. Proc.* Vol. 1. Alan R. Liss, New York, 1983, pp. 67-95.
3. Redman, J., Deep shaft treatment for sewage. *Chemical Engineer (Lond.)*, **441** (1987) 12-13.
4. Varey, P., Airlift for purity. *Chemical Engineer (Lond.)*, **529** (1992) s37.
5. Chisti, Y. & Moo-Young, M. Airlift bioreactors for treatment of hydrocarbon contaminated wastes. In *Better Living Through Biochemical Engineering*, eds W. K. Teo, M. G. S. Yap & S. K. W. Oh. University of Singapore, Singapore, 1994, pp. 771-6.
6. Moo-Young, M. & Chisti, Y., Bioreactor applications in waste treatment. *Res. Cons. Recycl.*, **11** (1994) 13-24.
7. Chisti, Y. & Moo-Young, M., Improve the performance of airlift reactors. *Chem. Eng. Progress*, **89**(6) (1993) 38-45.
8. Chisti, Y. & Moo-Young, M., Hydrodynamics and oxygen transfer in pneumatic bioreactor devices. *Biotechnol. Bioeng.*, **31** (1988) 487-94.
9. Rand, M. C., Greenberg, A. E. & Taras, M. J. (eds), *Standard Methods for the Examination of Water and Wastewater*, 14th edn. American Public Health Association, Washington, 1975, p. 87.
10. Chisti, Y. & Moo-Young, M., Airlift reactors: Characteristics, applications and design considerations. *Chem. Eng. Commun.*, **60** (1987) 195-242.
11. Fan, L. S., Hwang, S. J. & Matsuura, A., Hydrodynamic behaviour of a draft tube gas-liquid-solid spouted bed. *Chem. Eng. Sci.*, **39** (1984) 1677-88.
12. Chisti, Y. & Moo-Young, M., Gas holdup in pneumatic reactors. *Chem. Eng. J.*, **38** (1988) 149-52.